

<sup>1</sup> Study of neutrino-nucleus interaction at around 1 GeV using  
<sup>2</sup> a 3D grid-structure neutrino detector, WAGASCI at J-PARC  
<sup>3</sup> neutrino monitor hall

<sup>4</sup> A. Bonnemaison, R. Cornat, L. Domine, O. Drapier, O. Ferreira, F. Gastaldi,  
<sup>5</sup> M. Gonin, J. Imber, M. Licciardi, F. Magniette, T. Mueller, L. Vignoli, and O. Volcy

<sup>6</sup> *Ecole Polytechnique, IN2P3-CNRS, Laboratoire Leprince-Ringuet, Palaiseau,  
7 France*

<sup>8</sup> S. Cao and T. Kobayashi

<sup>9</sup> *High Energy Accelerator Research Organization (KEK), Tsukuba, Ibaraki, Japan*

<sup>10</sup> M. Khabibullin, A. Khotjantsev, A. Kostin, Y. Kudenko, A. Mefodiev, O. Mineev,  
<sup>11</sup> S. Suvorov, and N. Yershov

<sup>12</sup> *Institute for Nuclear Research of the Russian Academy of Sciences, Moscow, Russia*

<sup>13</sup> B. Quilain

<sup>14</sup> *Kavli Institute for the Physics and Mathematics of the Universe (WPI), The  
15 University of Tokyo Institutes for Advanced Study, University of Tokyo, Kashiwa,  
16 Chiba, Japan*

<sup>17</sup> T. Hayashino, A. Hiramoto, A.K. Ichikawa, K. Nakamura, T. Nakaya, K Yasutome,  
<sup>18</sup> and K. Yoshida

<sup>19</sup> *Kyoto University, Department of Physics, Kyoto, Japan*

<sup>20</sup> Y. Azuma, J. Harada, T. Inoue, K. Kin, N. Kukita, S. Tanaka, Y. Seiya,  
<sup>21</sup> K. Wakamatsu, and K. Yamamoto

<sup>22</sup> *Osaka City University, Department of Physics, Osaka, Japan*

23 A. Blondel, F. Cadoux, Y. Karadzhov, Y. Favere, E. Noah, L. Nicola, S. Parsa, and  
24 M. Rayner

25 *University of Geneva, Section de Physique, DPNC, Geneva, Switzerland*

26 N. Chikuma, F. Hosomi, T. Koga, R. Tamura, and M. Yokoyama

27 *University of Tokyo, Department of Physics, Tokyo, Japan*

28 Y. Hayato

29 *University of Tokyo, Institute for Cosmic Ray Research, Kamioka Observatory,  
30 Kamioka, Japan*

31 Y. Asada, K. Matsushita, A. Minamino, K. Okamoto, and D. Yamaguchi

32 *Yokoyama National University, Faculty of Engineering, Yokoyama, Japan*

33 December 7, 2017

34 **1 Introduction**

35 The understanding of neutrino-nucleus interactions in the 1 GeV energy region is critical  
36 for the success of accelerator-based neutrino oscillation experiments such as the T2K exper-  
37 iment. Complicated multi-body effects of nuclei render this understanding difficult. The  
38 T2K near detectors have been measuring these and significant progress has been achieved.  
39 However, the understanding is still limited. One of the big factors preventing from full  
40 understanding is the non-monochromatic neutrino beam spectrum. Measurements with  
41 different but some overlapping beam spectra would greatly benefit to resolve the contri-  
42 bution from different neutrino energies. We, the Wagasci collaboration, proposes to study  
43 the neutrino-nucleus interaction at the B2 floor of the neutrino monitor building, where  
44 different neutrino spectra can be obtained due to the different off-axis position. Our experi-  
45 mental setup contains 3D grid-structure plastic-scintillator detectors filled with water as the  
46 neutrino interaction target (Wagasci modules), two side- and one downstream- muon range  
47 detectors(MRD's). The 3D grid-structure and side-MRD's allows a measuremen of wider-  
48 angle scattering than the T2K off-axis near detector (ND280). High water to scitillator  
49 material ratio enables the measurement of the neutrino interaction on water, which is higly  
50 desired for the T2K experiment because it's far detector, Super-Kamiokande, is composed

51 of water. The MRD's consist of plastic scintillators and iron plates. The downstream-  
52 MRD, so called the Baby MIND detector, is also work as a magnet and provides the  
53 charge identification capability. The charge identification is essentially important to select  
54 antineutrino events in the antineutrino beam because contamination of the neutrino events  
55 is as high as 30%. Most of the detectors has been already constructed and commissioned as  
56 the J-PARC T59 experiment. Therefore, the collaboration will be ready to proceed to the  
57 physics data daking for the T2K beam time in January 2019. We will provide the cross sec-  
58 tions of the charged current neutrino and antineutrino interactions on water with slightly  
59 higher neutrino energy than T2K ND280 with wide angler acceptance. When combined  
60 with ND280 measurements, our measurement would greatly improve the understanding of  
61 the neutrino interaction at around 1 GeV and contribute to reduce the most significant  
62 uncertainty of the T2K experiment.

## 63 **2 Experimental Setup**

64 Figure. 1 shows a schematic view of the entire set of detectors. A central detector, Wagasci  
65 modules, consists of 3D grid-structure plastic-scintillator detectors filled with water as the  
66 neturino interaction target. They are surrounded by two side- and one downstream- muon  
67 range detectors(MRD's) The MRD's are used to select muon tracks from the charged-  
68 current (CC) interactions and to reject short tracks caused by neutral particles that orig-  
69 inate mainly from neutrino interactions in material surrounding the central detector, like  
70 the walls of the detector hall, neutrons and gammas, or neutral-current (NC) interactions.  
71 The muon momentum can be reconstructed from its range inside the detector. The MRD's  
72 consist of plastic scintillators and iron plates. In addition, eaco of the iron plates of the  
73 downstream-MRD, so called the Baby MIND detector, is wound by a coil and can be  
74 magnetized. It provide the charge selection capability.

75 For all detectors, scintillation light in the scintillator bar is collected and transported  
76 to a photodetector with a wavelength shifting fiber (WLS fiber). The light is read out by  
77 a photodetector, Multi-Pixel Photon Counter (MPPC), attached to one end of the WLS  
78 fiber. The signal from the MPPC is read out by the dedicated electronics developed for the  
79 test experiment to enable bunch separation in the beam spill. The readout electronics is  
80 triggered using the beam-timing signal from MR to synchronize to the beam. The beam-  
81 timing signal is branched from those for T2K, and will not cause any effect on the T2K  
82 data taking.

83 T2K adopted the off-axis beam method, in which the neutrino beam is intentionally  
84 directed 2.5 degrees away from SK producing a narrowband  $\nu_\mu$  beam. The off-axis near  
85 detector, ND280, is installed towards the SK direction in the B1 floor of the near detector  
86 hall of the J-PARC neutrino beam-line. We propose to install our detector in the B2 floor  
87 of the near detector hall, where the off-axis angle is similar but slightly different. The  
88 candidate detector position in the B2 floor is shown in Fig. 2. The expected neutrino

tmp.pdf

Figure 1: Schematic view of entire sets of detectors.

89 energy spectrum at the candidate position is shown in Fig. 3.

90 **2.1 Wagasci module**

91 The dimension of the central detector is 100cm  $\times$  100cm in the x and y directions and  
92 200cm along the beam direction. The total water and hydrocarbon masses serving as  
93 neutrino targets are  $\sim$ 1 ton each. Inside the central detector, plastic scintillator bars are  
94 aligned as a 3D grid-like structure, shown in Fig. 4, and spaces in the structure are filled  
95 with the neutrino target materials, water and hydrocarbon. When neutrinos interact with  
96 hydrogen, oxygen or carbon, in water and hydrocarbon, charged particles are generated.  
97 Neutrino interactions are identified by detecting tracks of charged particles through plastic  
98 scintillation bars. Thanks to the 3 D grid-like structure of the scintillator bars, the central  
99 detector has  $4\pi$  angular acceptance for charged particles. Furthermore, adopting a 2.5cm  
100 grid spacing, short tracks originated from protons and charged pions can be reconstructed  
101 with high efficiency. Thin plastic scintillator bars (thickness  $\sim$  0.3cm) will be used for the  
102 central detector to reduce the mass ratio of scintillator bars to neutrino target materials,  
103 because neutrino interactions in the scintillator bars are a background for the cross section  
104 measurements. Scintillator bars whose dimensions are 2.5cm x 0.3cm x 100cm will be used  
105 for the central detector. The total number of channels in the central detector is 12880.

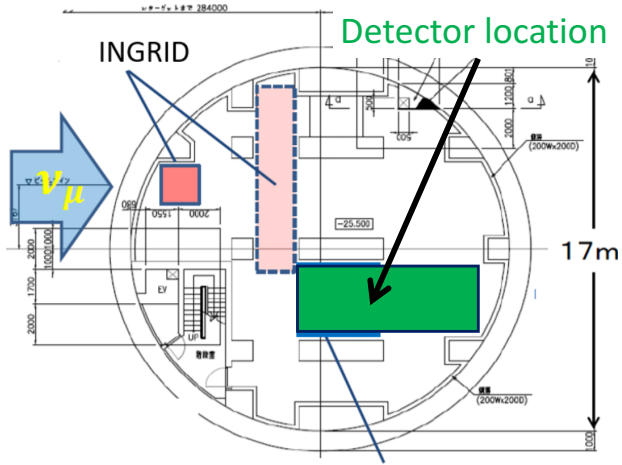


Figure 2: Candidate detector position in the B2 floor of the near detector hall.

<sup>106</sup> **2.2 Baby MIND**

<sup>107</sup> **2.3 Side muon range detector**

<sup>108</sup> Four Side-MRD modules for tracking secondary particles from neutrino interactions will  
<sup>109</sup> be constructed by the end of January 2018. Each Side-MRD module is composed of 11  
<sup>110</sup> steel plates and 10 layers of total 80 scintillator slabs installed in 13 mm gaps between the  
<sup>111</sup> 30 mm thick plates. Each steel plate size is  $30 \times 1610 \times 1800$  mm<sup>3</sup>. Total module size is  
<sup>112</sup>  $2236 \times 1630 \times 975$  mm<sup>3</sup> as shown in Fig. 5, weight is  $\sim 8.5$  ton.

<sup>113</sup> Scintillator bars were manufactured by Uniplast company in Vladimir, Russia. Polystyrene  
<sup>114</sup> based scintillators were extruded with thickness of 7 mm, then cut to the size of  $7 \times 200 \times$   
<sup>115</sup> 1800 mm<sup>3</sup>. Dopant composition is 1.5% PTP and 0.01% POPOP. Scintillator surface was  
<sup>116</sup> etched by a chemical agent to form a white diffuse layer with excellent reflective perfor-  
<sup>117</sup> mance. Ideal contact between the scintillator and the reflector raises the light yield up to  
<sup>118</sup> 50% comparing to an uncovered scintillator. Sine like groove was milled along the scin-  
<sup>119</sup> tillator to provide uniform light collection over the whole scintillator surface. WLS Y11  
<sup>120</sup> Kuraray fiber of 1 mm diameter is glued with an optical cement EJ-500 in the S-shape  
<sup>121</sup> groove as shown in Fig. 6. Bending radius is fixed to 30 mm that was specified to be safe  
<sup>122</sup> for Kuraray S-type fibers. Both ends of the fiber are glued into optical connectors (Fig. 7)  
<sup>123</sup> which mounted within a scintillator body.

<sup>124</sup> The plastic molded connectors provide an interface to SiPMs, Hamamatsu MPPC  
<sup>125</sup> S13081-050CS(X1) used for the WAGASCI detector. Optical coupler of this type (so-called  
<sup>126</sup> Baby-mind type of optical connector) consists of two parts (see Fig. 7): an container for

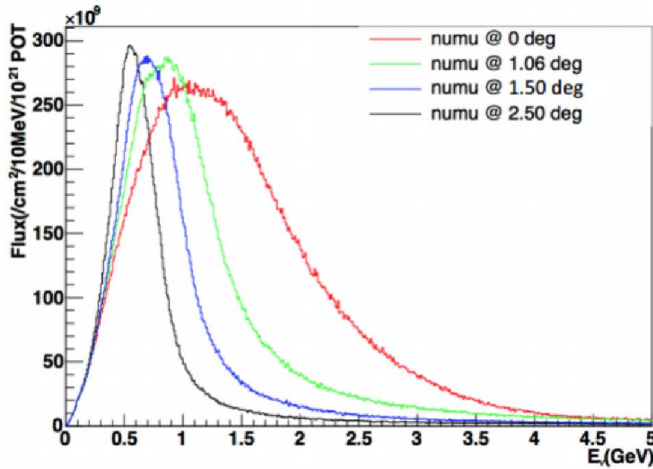


Figure 3: Neutrino energy spectrum at the candidate detector position(red). The spectrum at the ND280 site (black) is also shown.

the MPPC and a ferrule with the fiber. The ferrule is glued in the scintillator, and its end with glued in WLS fiber was polished. Both parts of the optical coupler are latched by a snap-like mechanism: a locking groove inside the container and matching ring protuberance on the ferrule. To ensure the optical contact a foam spring made of sponge rubber presses the MPPC to the fiber end (Fig. 8).

Scintillators for the Side-MRD modules had been assembled at INR in Russia, and shipped to Japan in July 2017. The light yield for each scintillator was measured with cosmic rays at INR and at YNU in Japan after delivery. Parameters measured at the center of the counter were : the light yields  $LY_1$  and  $LY_2$  at both ends, the light yield asymmetry between the ends calculated as  $100\% \times \frac{LY_1 - LY_2}{LY_1 + LY_2}$ . After tests at INR we selected 324 counters from measured 332 ones with the mean light yield of 45 p.e./MIP ( $LY_1 + LY_2$ ) and the asymmetry value less than 10 %. The measurements at YNU yielded the average total light yield of about 40 p.e./MIP which varies in range from 32 to 50 p.e./MIP (Fig. 9 (left)). Only two counters showed relatively high asymmetry close to 25 % as shown in Fig. 9 (right). Using the results of the quality assurance test we selected 320 scintillator counters for the Side-MRD modules.

We also measured the time resolution for a combination of four counters piled each on another one. Time resolution for a single counter is determined as rms of  $(T_{left} - T_{right})/2$  distribution. The difference of times was chosen to remove the correlated time fluctuation caused by a start trigger signal. The average result for four counters is  $\sigma_T = 1.04$  ns (Upper left plot in Fig. 10). For a set of  $n$  counters the time resolution is calculated as

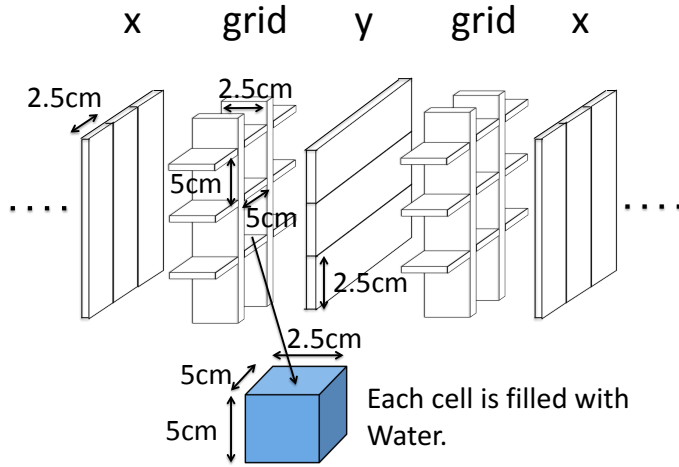


Figure 4: Schematic view of 3D grid-like structure of plastic scintillator bars inside the central detector.

<sup>148</sup>  $\frac{(T_L - T_R)_1 + (T_L - T_R)_2 + \dots + (T_L - T_R)_n}{2 \times n}$ . The result of combination of 2, 3, 4 counters is 0.79 ns,  
<sup>149</sup> 0.66 ns and 0.58 ns, correspondently (Fig. 10).

<sup>150</sup> Construction of Side-MRD modules will be done from November 2017 to January 2018  
<sup>151</sup> at Yokohama National University, then they will be transported to J-PARC and will be  
<sup>152</sup> installed at B2 floor of the T2K near detector hall before T2K beam in March 2018.

### <sup>153</sup> 3 Physics goals

<sup>154</sup> We will measure the differential cross section for the charged current interaction on H<sub>2</sub>O  
<sup>155</sup> and/or CH. The water-scintillator mass ratio of the Wagasci module is as high as 5:1 and  
<sup>156</sup> the high purity measurement of the cross section on H<sub>2</sub>O is possible. One experimental  
<sup>157</sup> option is to replace one of the two Wagasci module with the T2K proton module which is  
<sup>158</sup> fully made with plastic scintillators. It will allow the precise comparison of cross section  
<sup>159</sup> between H<sub>2</sub>O and CH and also comparison of cross sections with ND280. Another option  
<sup>160</sup> is to remove water from one of the two Wagasci module. The water-out WAGASCI module  
<sup>161</sup> will make it possible to measure wider- angle scatterings for CH target and will provide a  
<sup>162</sup> low density medium for the detection of low momentum protons. The water-out WAGASCI  
<sup>163</sup> data also can be used to subtract the background from interaction with scintillators in the  
<sup>164</sup> water target measurement . Our setup would allow the measuemrents of inclusive and  
<sup>165</sup> also exclusive channles such as 1- $\mu$ , 1- $\mu 1p$ , 1- $\mu 1\pi \pm np$  samples, former two of which are  
<sup>166</sup> mainly caused by the quasi-elastic and 2p2h interaction and the latter is mainly caused by

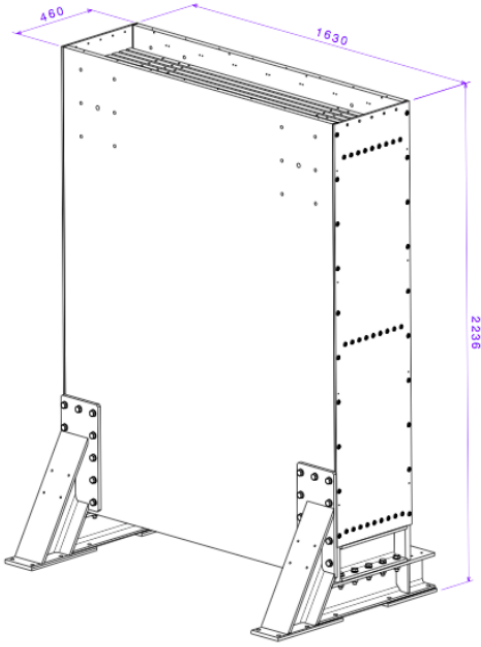


Figure 5: Support structure of the Side-MRD module.

167 resonant or coherent pion production and deep elastic scattering. In general, an accelerator  
 168 produced neutrino beam spectrum is wide and the energy reconstruction somehow rely on  
 169 the neutrino interaction model. Therefore, recent neutrino cross section measurement  
 170 results including T2K are given as a flux-integrated cross section rather than cross sections  
 171 as a function of the neutrino energy to avoid the model dependency. We can provide  
 172 the flux-averaged cross section. In addition, by combining our measurements with those at  
 173 ND280, model-independent extraction of the cross section for narrow energy region becomes  
 174 possible. This method was demonstrated in ?? and also proposed by P\*\* (NUPRISM).  
 175 add Yasutome plot here or later.

### 176 3.1 Expected number of events

177 Expected number of neutrino events after the event selections is evaluated with Monte  
 178 Carlo simulations as we will discuss in Section 6.  $2.41 \times 10^4$  CC events are expected in  
 179 two WAGASCI modules after the selection with  $1 \times 10^{20}$  POT in neutrino-mode, and its  
 180 purity is 75.5 %. In case we choose the option with one WAGASCI module and the T2K  
 181 proton module,  $1.2 \times 10^4$  CC events are expected in the WAGASCI module and  $\sim 1 \times 10^4$   
 182 CC events are expected in the T2K proton module. In case we choose the option with one

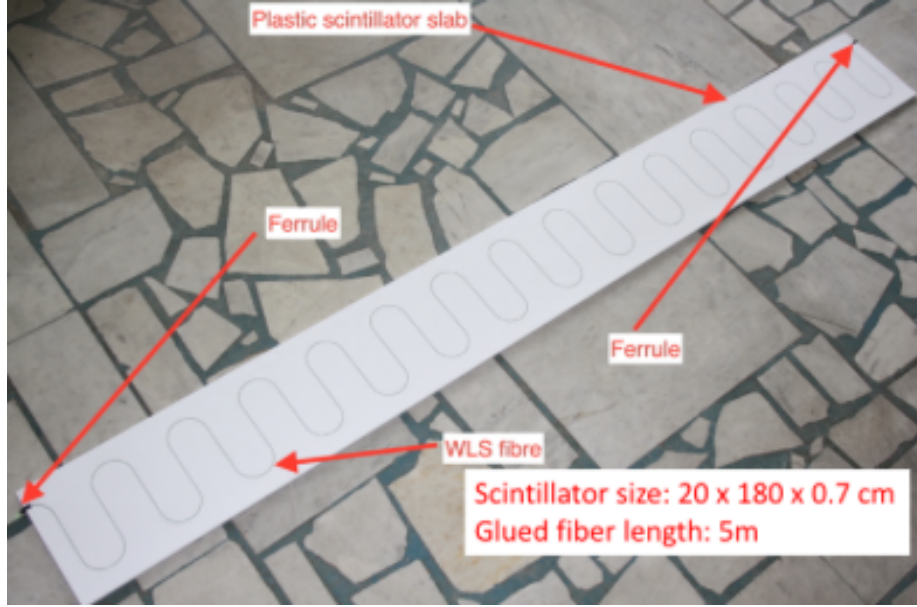


Figure 6: Scintillator bar of the Side-MRD modules.

<sup>183</sup> water-in WAGASCI module and one water-out WAGASCI module,  $1.2 \times 10^4$  CC events are  
<sup>184</sup> expected in the water-in module and  $0.24 \times 10^4$  CC events are expected in the water-out  
<sup>185</sup> module.

### <sup>186</sup> 3.2 Nuclear effects

<sup>187</sup> In T2K experiment, neutrinos interact with bound nucleons in relatively heavy nuclei  
<sup>188</sup> (Carbon and Oxygen), so the cross-section is largely affected by nuclear effects. The nuclear  
<sup>189</sup> effects are categorized as nucleons' momentum distribution in nucleus, interactions with  
<sup>190</sup> correlated pairs of nucleons in nucleus (two particles-two holes, 2p2h), collective nuclear  
<sup>191</sup> effects calculated with Random Phase Approximation (RPA) and final state interactions  
<sup>192</sup> (FSI) of secondary particles in the nuclei after the initial neutrino interactions.

<sup>193</sup> The 2p2h interactions mainly happen through  $\Delta$  resonance interactions following a  
<sup>194</sup> pion-less decay and interactions with a correlated nucleon pair. The 2p2h interactions are  
<sup>195</sup> observed in electron scattering experiments (add ref. here) where the 2p2h events observed  
<sup>196</sup> in the gap between Quasi-Elastic region and Pion-production region as shown in Fig. ??.  
<sup>197</sup> Neutrino experiments also attempt to measure the 2p2h interactions, but separation of the  
<sup>198</sup> QE peak and the 2p2h peak is more difficult because transferred momentum ( $p$ ) and energy

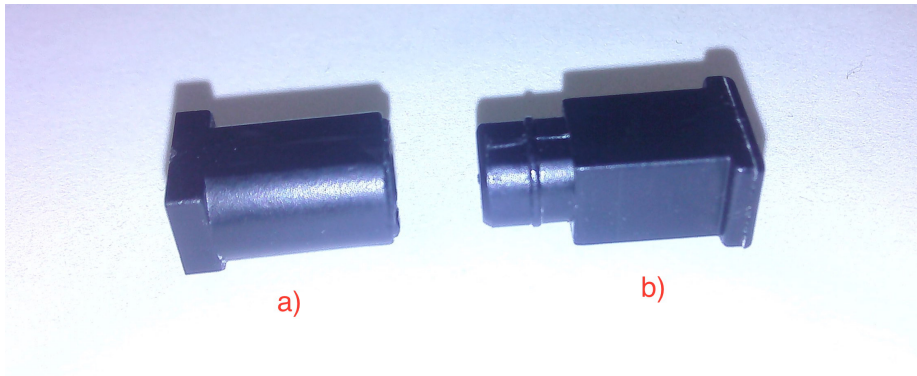


Figure 7: Optical connector for the Side-MRD scintillator. a) MPPC cover. b) Ferrule.

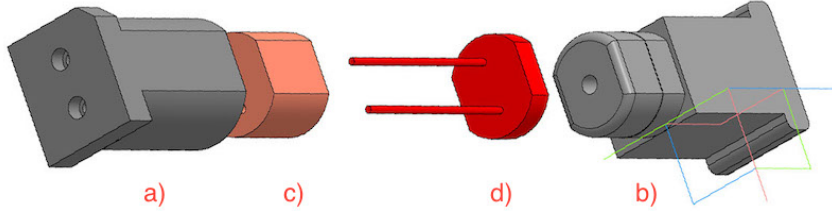


Figure 8: Scheme of the MPPC placement in optical connector. a) MPPC cover. b) Ferrule. c) Spring (sponge rubber). d) MPPC.

(w) are largely affected by neutrino energies which cannot be determined event-by-event in the wide energy spectrum of the accelerator neutrino beam. Our model-independent narrow neutrino spectra extracted from combined analyses of our data and ND280 data are ideal for searching the 2p2h interaction because clearer separation of the QE peak and the 2p2h peak is expected. Another way to observe the 2p2h interaction is direct measurement of proton tracks in CC $0\pi$  sample with low detection threshold and full acceptance. Fig. ?? shows proton multiplicities in CCQE events and 2p2h events, and Fig. ?? shows opening angles among two proton tracks in the same samples. The water-out WAGASCI can provide good sample for the 2p2h interaction search because its low density medium enables the detection of low momentum protons in addition to the full acceptance.

The corrections from collective nuclear effects calculated by RPA as a function of  $Q^2$  are shown in Fig. ???. The  $Q^2$  dependence of the correction can be tested by measuring angular distribution of muons in CC1- $\mu$  and CC1- $\mu 1p$  events. The uncertainties of the corrections in low (high)  $Q^2$  regions can be constrained by observing the events with a forward-going

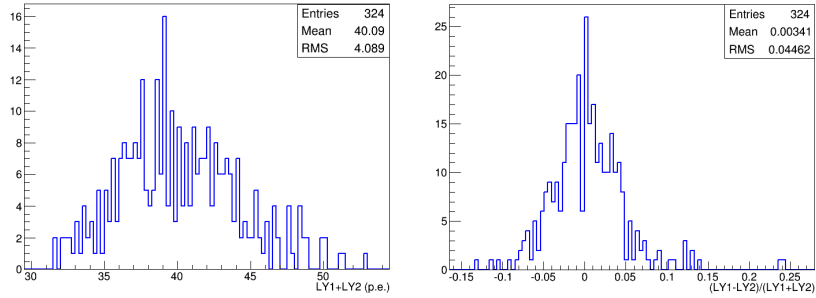


Figure 9: Total light yield distribution (left) and light yield assymetry (right) measured at YNU.

213 (high-angle) muon, so it is essential to measure muon tracks with full acceptance.

214 T2K experiment is starting to use  $\nu_e$  CC1 $\pi$  events for its CP violation search to increase  
 215 the statistics. One of the biggest uncertainty of the CC1 $\pi$  sample comes from the final  
 216 state interactions of pions in the nuclei after the initial neutrino interactions because they  
 217 change the multiplicity, charge and kinematics of the pions. The multi-pion production  
 218 events can be migrated into the CC1 $\pi$  sample due to the FSIs, and they become important  
 219 backgrounds. We can constrain the uncertainties from the pion FSIs by measuring pion  
 220 rescattering in the detector and pion multiplicity in  $\nu_\mu$  CCn $\pi$  sample with low detection  
 221 threshold and full acceptance for pion tracks. The water-out WAGASCI can provide good  
 222 sample for the pion FSI studies because its low density medium enables the detection of  
 223 low momentum pions in addition to the full acceptance.

## 224 4 Status of J-PARC T59 experiment

225 We had submitted a proposal of a test experiment to test a new detector with a water  
 226 target, WAGASCI, at the T2K near detector hall to J-PARC PAC on April 2014, and the  
 227 proposal was approved as J-PARC T59. There are several updates on the project after  
 228 three years from then. Fist, the start time of neutrino beam measurement is changed from  
 229 December 2015 to October 2017, and the requested neutrino beam is changed from  $1 \times 10^{21}$   
 230 POT of  $\nu$  beam to  $0.8 \times 10^{21}$ POT of anti- $\nu$  beam. Second, the detector configuration is  
 231 changed. In the original proposal, central neutrino detector are expected to be surrounded  
 232 by newly developed muon-range detectors (MRDs), but we will use spare neutrino detectors  
 233 of the T2K experiment instead of them during neutrino beam measurement from October  
 234 to December 2017. Construction of the newly developed MRDs, Baby-MIND and Side-  
 235 MRD, is in progress, and they will be installed to the both sides and the downstream of  
 236 the central neutrino detector from January to March 2018. Then, we will resume neutrino

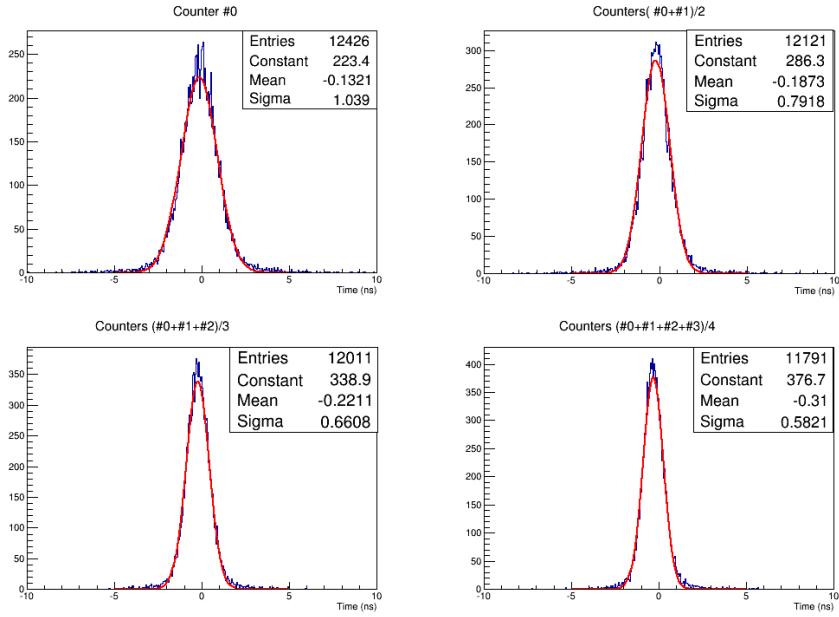


Figure 10: Time resolution for one (upper left) and a set of 2,3,4 Side-MRD counters.

beam measurements from March 2018 and will take the neutrino beam data until May 2018.

#### 4.1 On-axis beam measurement with Prototype detector

Add INGRID water module measurement here.

#### 4.2 Plans from October 2017 to May 2018

J-PARC MR will extract its proton beam to T2K neutrino beam-line from October to December 2017, and, from March to May 2018. T2K experiment will produce anti-neutrino beam and will accumulate  $\sim 8 \times 10^{20}$  POT data during the above period.

J-PARC T59 will perform neutrino beam measurements on the B2 floor of the T2K near neutrino detector hall during the above period to test basic performances of the WAGASCI detector and new electronics. During the beam measurements from October to December 2017, one WAGASCI module will be placed between spare neutrino detectors of the T2K experiment, INGRID Proton module and INGRID standard module. Here, the INGRID Proton module is used as a charged particle VETO detector and, the INGRID standard module is used as a downstream muon detector. We had submitted a proposal

252 to use these spare neutrino detectors for the T59 neutrino beam measurements to the T2K  
253 collaboration, and we got an approval from T2K.

254 During the beam measurements from March to May 2018, Baby-MIND and two side  
255 muon-range detector (Side-MRD) modules will be installed on the downstream and the  
256 both sides of the WAGASCI detector, as shown in Fig. 11, to increase angular acceptance  
257 for secondary charged particles from neutrino interactions. Add Baby-MIND commission-  
258 ing items here!!!

tmp.pdf

Figure 11: J-PARC T59 detector configuration with Baby-MIND and two Side-MRD modules from Mar. to May 2018. (Need to prepare the figure.)

259 Expected number of neutrino events in the WAGASCI detector during the above beam  
260 period is evaluated with Monte Carlo simulations. Neutrino beam flux at the detector  
261 location is simulated by T2K neutrino flux generator, JNUBEAM, neutrino interactions  
262 with target materials are simulated by a neutrino interaction simulator, NEUT, detector  
263 responses are simulated using GEANT4-based simulation. The neutrino flux at the detector  
264 location, 1.5 degrees away from the J-PARC neutrino beam axis, is shown in Figure 3, and  
265 its mean neutrino energy is around 0.68 GeV. An event display of the GEANT4-based  
266 detector simulation is shown in Figure 14.

267 To perform the detector performance test, the following event selections are applied to  
268 the data. First, track reconstructions are performed in the WAGASCI detector, and the  
269 reconstructed vertex is required to be inside a defined fiducial volume,  $80 \times 80 \times 32 \text{ cm}^3$   
270 region at the center of the detector, to reduce contamination from external backgrounds.  
271 Second, at least one charged particle is required to reach to INGRID standard module  
272 or Side-MRD modules, and it makes more than two hits in these sub-detectors. With the

273 event selection, expected numbers of the neutrino-candidate events during the beam period  
274 are summarized in Table 1. Using the data, we will test the detector performance with  
275  $\sim 3\%$  statistical uncertainties.

## 276 5 Detector performance

### 277 5.1 Wagasci module

278 To demonstrate the performance of the Wagasci module and also to study the neutrino  
279 interaction, the first Wagasci module was installed at the on-axis position, in front of  
280 the T2K INGRID horizontal center module in 2016. The INGRID module is made of iron  
281 plates and segmented plastic scintillator bars. It's cross sectional size viewed from the beam  
282 direction is  $1 \text{ m} \times 1 \text{ m}$ . The charged current interactions in the Wagasci module are selected  
283 by requiring a muon track candidate in the INGRIRD modules. Here, we describe the  
284 performance of the Wagasci module evaluated at this T2K on-axis measurement. Figure 12  
285 shows the light yeild of channels for muons produced by the interaction of neutrinos in the  
hall wall. The light yield is sufficiently hgih to get good hit efficieincy. A track search

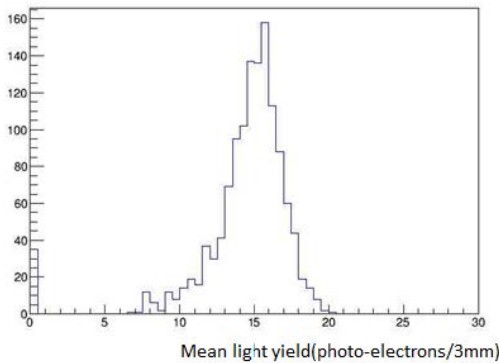


Figure 12: Light yield of channels for muons produced by the interaction of neutrinos in the hall wall.

286  
287 algorithm based on the cellular automaton has been developed using the software tools by  
288 the T2K INGRID. The tracking efficiency in 2-dimentional projected plane was evalualted  
289 by comparing the reconstructed track in the Wagasci module and the INGRID module and  
290 shown in Fig.13. Note that that the tracking efficinency for high angle ( $> 70 \text{ deg}$ ) is not  
291 evaluated because of the acceptance of the INGRID module, not because of the limitation  
292 of the Wagasci module.

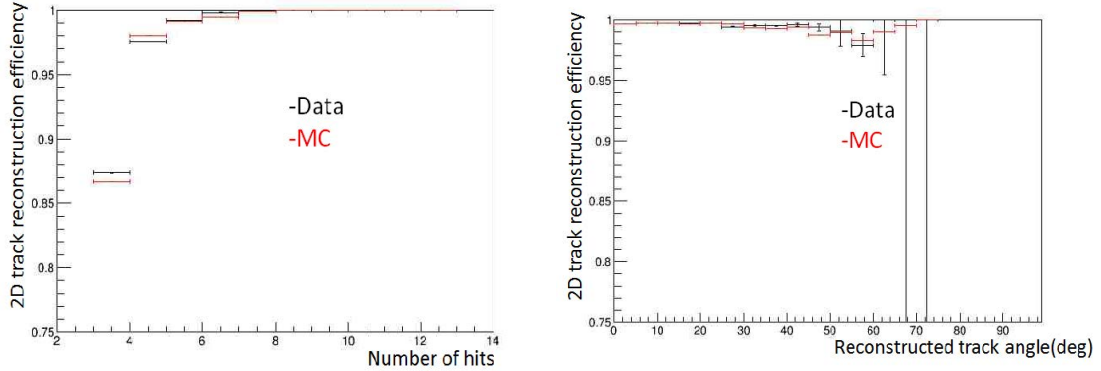


Figure 13: 2D track reconstruction efficiency as a function of number of hits (left) and track angle (right). Here the track angle is the one reconstructed by the INGRID module.

293 **5.2 Baby MIND**

294 **5.3 Side muon range detector**

295 **6 MC studies**

296 **6.1 Detector simulation**

297 Expected number of neutrino events in the WAGASCI detector is evaluated with Monte  
 298 Carlo simulations. Neutrino beam flux at the detector location is simulated by T2K neutrino  
 299 flux generator, JNUBEAM, neutrino interactions with target materials are simu-  
 300 lated by a neutrino interaction simulator, NEUT, detector responses are simulated using  
 301 GEANT4-based simulation. The neutrino flux at the detector location, 1.5 degrees away  
 302 from the J-PARC neutrino beam axis, is shown in Figure 3, and its mean neutrino energy  
 303 is around 0.68 GeV.

304 **6.1.1 Detector geometry**

305 The detector geometry in the GEANT4-based simulation is slightly different from the  
 306 actual detector as shown in Fig. 16. The active neutrino target region consists of four  
 307 WAGASCI modules, and each WAGASCI detector has the dimension with 100 cm  $\times$  100  
 308 cm in the x and y directions and 50 cm along the beam direction. An event display of a  
 309 MC event in the WAGASCI detectors is shown in Figure ???. Two Side-MRD modules is  
 310 installed at both sides of the WAGASCI modules, and each Side-MRD module consists of  
 311 ten iron plates whose dimension is 3 cm (thickness)  $\times$  180 cm (height)  $\times$  320 cm (width).  
 312 The distance between the Side-MRD modules and WAGASCI modules is 60 cm. The

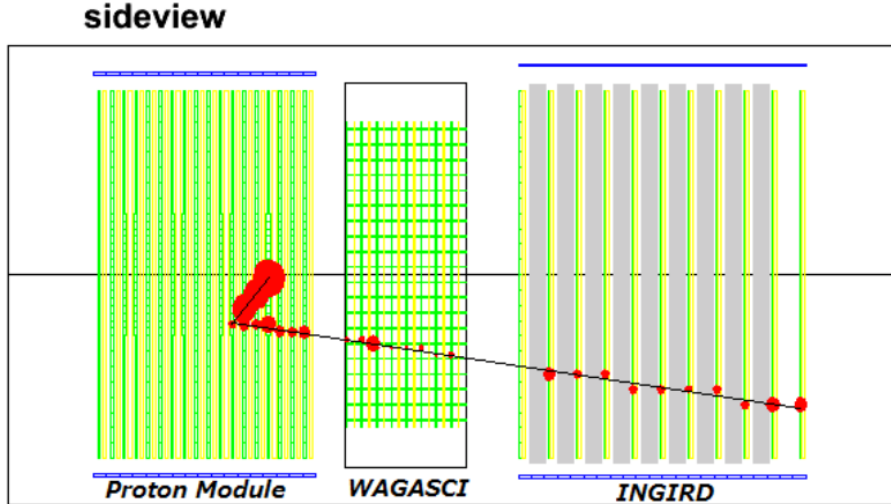


Figure 14: J-PARC T59 event display of a neutrino event in the GENAT4-based detector simulation.

313 downstream-MRD equivalent to the Baby-MIND is installed at the downstream of the  
 314 WAGASCI modules. The downstream-MRD consists of ten iron plates whose dimension is  
 315 3 cm (thickness)  $\times$  180 cm (height)  $\times$  320 cm (width) and another ten iron plates whose  
 316 dimension is 6 cm (thickness)  $\times$  180 cm (height)  $\times$  320 cm (width). The distance between  
 317 the downstream-MRD modules and WAGASCI modules is 60 cm.

318 In order to estimate backgrounds from neutrino interactions in the wall and floor of the  
 319 experimental hall, the geometry of the experimental hall is implemented in the GEANT4-  
 320 based detector simulation.

### 321 6.1.2 Response of detector components

322 The energy deposit inside the scintillator is converted into the number of photons. The  
 323 effects of collection and attenuation of the light in the scintillator and the WLS fiber are  
 324 simulated, and the MPPC response is also taken into account. The light yield is smeared  
 325 according to statistical fluctuations and electrical noise.

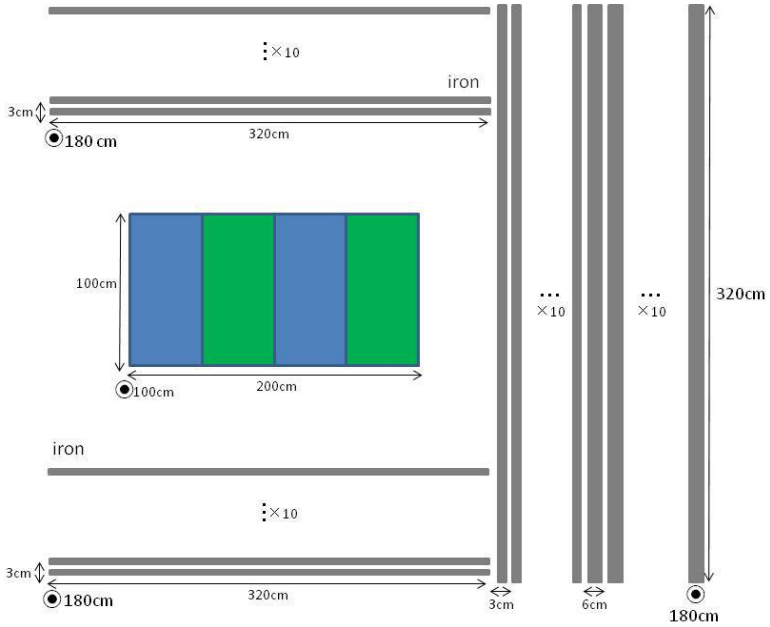


Figure 15: Geometry of the detectors in the Monte Carlo simulation.

## 326 6.2 Track reconstruction

327 To select neutrino interaction from the hit patterns, a track reconstruction algorithm is  
328 developed. The flow of the track reconstruction is as follows.

- 329     1. Two-dimensional track reconstruction in each sub-detectors
- 330     2. Track matching among the sub-detectors
- 331     3. Three -dimensional track reconstruction

332 Add explanation about two-dim reco, track matching and three-dim reco here.

## 333 6.3 Event selection

334 First, the events with the track which starts in 5 cm from the wall of the WAGASCI module  
335 are rejected to remove the background from the outside.

336 Second, to reject backgrounds from NC and neutral particles, the longest tracks are  
337 required to penetrate more than one (five) iron plates in Side-MRD modules (Baby-MIND).

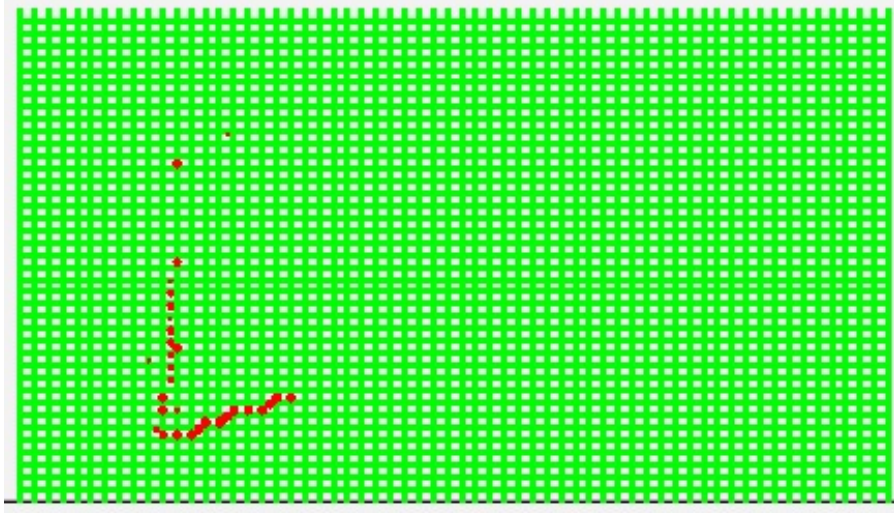


Figure 16: An event display of MC event in WAGASCI detectors. Green lines are scintillators and red circles are the hit channels.

Then, in order to measure muon momentum, the longest tracks are required to stop in MRDs (Side-MRD modules and Baby-MIND) or penetrate all iron plates.

Table 1 and 2 show numbers of the selected events after each event election in neutrino-mode and antineutrino-mode respectively. As for the neutrino-mode,  $2.12 \times 10^4$  CC events are expected with  $1 \times 10^{21}$  POT, and the purity is 81.3 %. The main background for the neutrino-mode is the neutrino interactions in the scintillators inside the WAGASCI detector. As for the antineutrino-mode,  $0.83 \times 10^4$  CC events are expected with  $1 \times 10^{21}$  POT, and the purity is 62.0 %. The main background for the antineutrino-mode is the wrong sign contamination from  $\nu_\mu$  events and the antineutrino interactions in the scintillators inside the WAGASCI detector.

Table 1: Expected number of the neutrino-candidate events in two WAGASCI modules after the event selections with  $1 \times 10^{21}$  POT in neutrino-mode.

Cut	CC	NC	Scinti Bkg.	Total
Reconstructed	45233	1749.27	9396.46	56378.8
FV	37876.8	1471.02	7869.57	47217.4
Pene. iron	28160.7	593.267	5750.79	34504.7
Stop/Penetrate MRDs	21195.4	534.914	4346.06	26076.4
after all cuts	81.3 %	2.1 %	16.7 %	100 %

Table 2: Expected number of the antineutrino-candidate events in two WAGASCI modules after the event selections with  $1 \times 10^{21}$  POT in antineutrino-mode.

Cut	CC	NC	Scinti Bkg.	Wrong sign bkg	Total
Reconstructed	16249.1	268.082	4468.83	5826.95	26813.0
FV	13644.7	223.211	3746.85	4866.36	22481.0
Pene. iron	10430.8	76.9422	2881.81	3901.35	17290.9
Stop/Penetrate MRDs	8328.73	71.2382	2240.59	2802.98	13443.5
after all cuts	62.0 %	0.5 %	16.7 %	20.9 %	100 %

348     Figure 17 and 18 show the reconstructed angles of the longest tracks in the selected  
 349     events in the neutrino-mode and the anti-neutrino mode respectively.

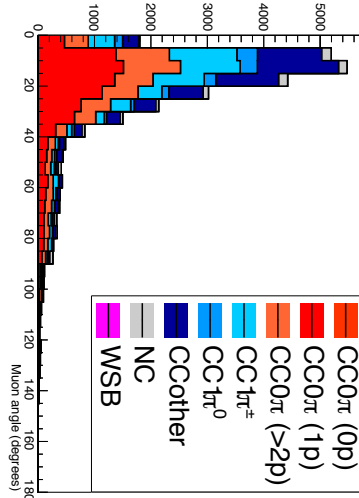


Figure 17: The reconstructed angles of the longest tracks in the selected events in the neutrino-mode.

350     Figure 19 and 20 show the iron plane numbers corresponding to the end points of the  
 351     longest tracks in the selected events.

#### 352     6.4 Cross section measurements on water

353     In the water target events, the background from interaction with scintillators has to be  
 354     subtracted by using the measurement of the hydrocarbon target.

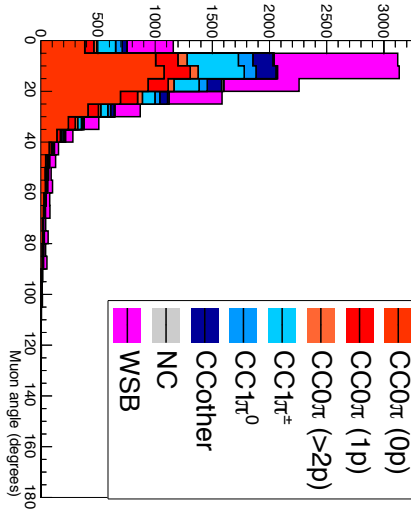


Figure 18: The reconstructed angles of the longest tracks in the selected events in the antineutrino-mode.

355    **6.4.1 Charged current cross section measurement**

356    **7 Standalone WAGASCI-module performances**

357    In the previous sections, the WAGASCI detector was studied using the Muon Range Detectors. In this section, the standalone abilities of WAGASCI module are presented. Using  
 358    the WAGASCI configuration presented in Section 6, we have evaluated that only 7% of  
 359    the muons will be stopped in one of the WAGASCI modules. THowever, this proportion  
 360    increases to 53% for pions and 73% for protons produced by neutrino interactions at  $1.5^\circ$   
 361    off-axis. Figure 21 shows the momentum distribution of these daughter particles as well as  
 362    for the sub-sample stopped in one of the WAGASCI modules. Therefore, the study of the  
 363    standalone abilities of the WAGASCI module in this section are dominantly motivated by:  
 364   

- 365    • the accurate measurement of the neutrino interaction final states. Though most of the  
   366    muons will be reconstructed and identified in the MRDs, the hadronic particles will  
   367    predominantly stops in one WAGASCI module. One has therefore to rely exclusively  
   368    on the WAGASCI module information alone to reconstruct, identify and measure the  
   369    momentum of pions or protons.
- 370    • the coverage of the MRDs is not  $4\pi$ . Using the WAGASCI module information can  
   371    therefore help to constraint the particles that exits the WAGASCI module but do

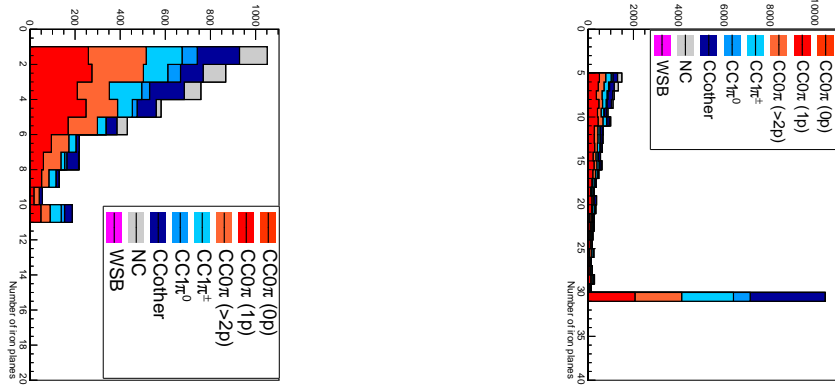


Figure 19: Iron plane numbers in Side-MRD (left) and Baby-MIND (right) corresponding to the end points of the longest tracks in the selected events in the neutrino-mode.

372 not geometrically enters any MRD.

- 373 • the particle identification of low momenta muons  $p_\mu < 300$  MeV/c that will leave only  
 374 few hits in the MRD. Using the WAGASCI module information will clearly enhance  
 375 the particle identification.

376 This study is based on an original study done for the ND280 upgrade target, with some  
 377 modifications. Though the cell size is similar to the WAGASCI configuration presented  
 378 in Section 6, the external dimensions are different ( $186.4 \times 60 \times 130$  cm $^3$ ). Whenever the  
 379 results are presented with this external size and this parameter is likely to impact the  
 380 result, it will be mentioned.

381 Note that in this section, a simplified reconstruction algorithm presented in Section 7.1 is  
 382 used. The fiducial volume is chosen accordingly as the inner cube of the module which  
 383 surfaces are distant of  $4 \times$  scintillator space = 10 cm from the module external surfaces.  
 384 The neutrino interactions are simulated using NEUT v5.3.2. The NEUT input neutrino  
 385 flux is estimated using JnuBeam v13a and assuming the detector to be located at  $1.5^\circ$   
 386 off-axis, as in Section 6. Note that the event reconstruction efficiency as a function of true  
 387 neutrino energy might be changed at  $1.5^\circ$ , due for example to different  $Q^2$  distributions. For  
 388 this reason, one has to note that the reconstruction results might slightly be changed from  
 389  $2.5^\circ$  and  $1.5^\circ$ . To avoid a similar change on the particle-only reconstruction efficiencies,  
 390 they will be presented as a function of variables that completely characterize the particle  
 391 kinematic state, *i.e.* its momentum and angle. Figure 22 shows the vertices distributions  
 392 of the daughter particles of neutrinos interacting one standard WAGASCI water-module.  
 393 In this section, we will show the detector reconstruction and particle identification in this  
 394 phase space, both for leptonic and hadronic particles. We will finally show an empty

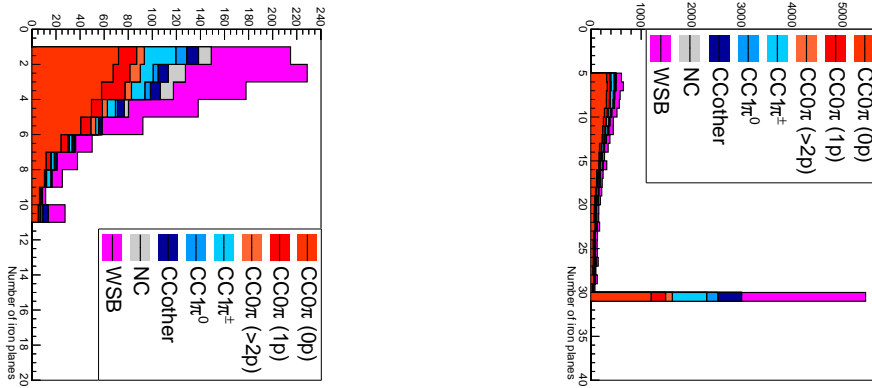


Figure 20: Iron plane numbers in Side-MRD (left) and Baby-MIND (right) corresponding to the end points of the longest tracks in the selected events in the antineutrino-mode.

395    WAGASCI module can highly enhance the ability to constrain the neutrino interaction  
 396    final state which is critical to reduce the corresponding uncertainties.

## 397    7.1 Reconstruction algorithm

### 398    7.1.1 Description

399    For this section, an ideal “simulated” reconstruction is developed. A particle is recon-  
 400    structed if:

- 401    1. The particle is charged.  
 402    2. Lets at least one hit (energy deposit  $> 2.5$  photo-electron) in a scintillator.  
 403

- 404    3. The particle enters one TPC and let one hit in the tracker.  
 405    Or

- 406
- 407    • The particle should be long enough to be reconstructed by the detector in at  
 408    least 2 out of 3 views (XZ, YZ, XY). The length criterion requires the particle  
 409    to let at least 4 hits in the detector. In the “less favourable case” of pure  
 410    longitudinal or transverse going tracks, it represents a the track length of  $L_{track} \geq$   
 411     $4 \times$  scintillator space = 10.0 cm.
  - 412    • In the views where particles pass the length criterion, the particle shall not  
 413    be superimposed with longer tracks in at least two views. The superposition

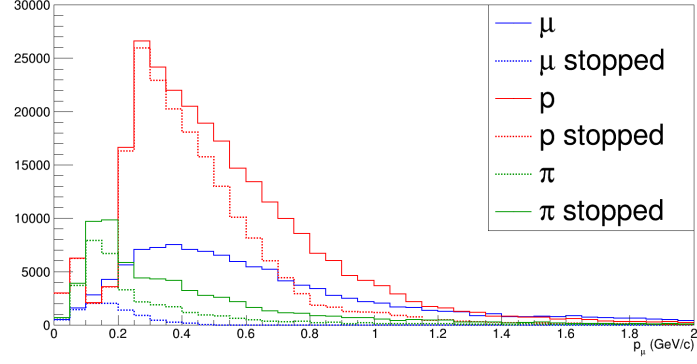


Figure 21: Momentum distribution of true particles in WAGASCI (plain) and corresponding distributions only for particles stopping into the WAGASCI module (dashed).

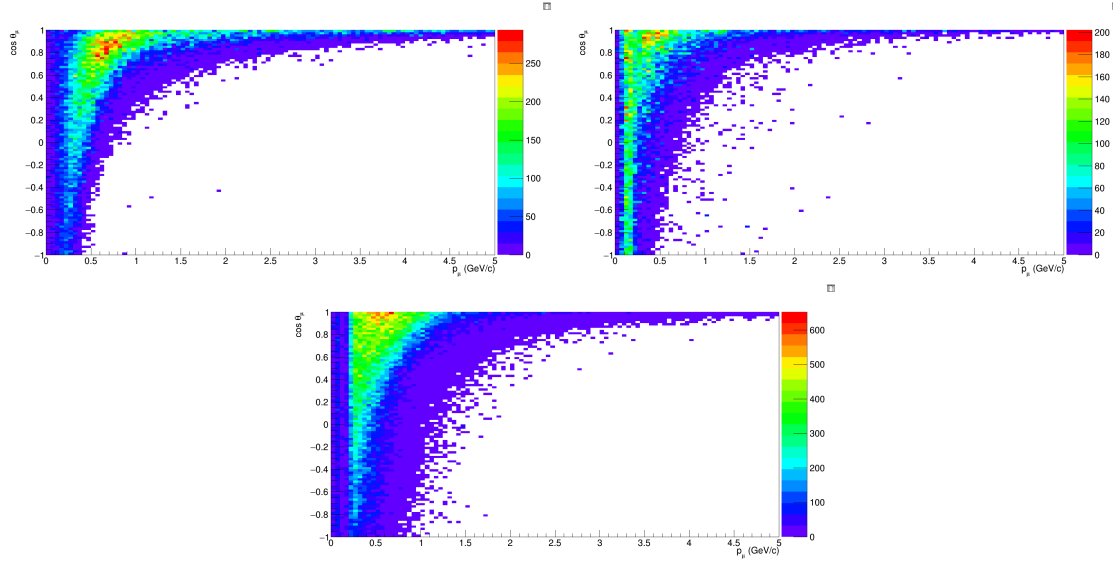


Figure 22: True number of muons (left), charged pions (right) and protons (bottom) in the two WAGASCI water-module as a function of the particles momenta and angles at  $1.5^\circ$ .

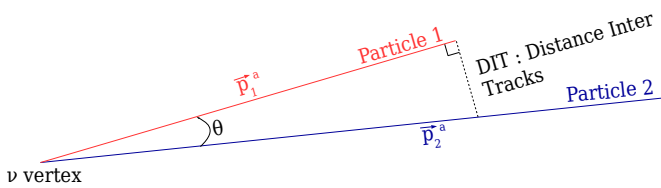


Figure 23: Definition of the distance inter tracks.

414 criterion is estimated with the distance inter-tracks (DIT) which corresponds to  
 415 the orthogonal distance between two tracks at the ending point of the shortest  
 416 one (see Figure 23). For a track 1, the superposition criterion is tested with  
 417 every longer tracks that starts at the same vertex. Let  $\vec{p}_1$  the vector of track  
 418 1, and  $p_1^a$  its projections in the XZ, YZ and XY planes respectively for  $i=1,2,3$ .  
 419 Note that these are projections in a 2D planes and not on a direction vector. In  
 420 this case, the relative angle between the track 1 and a longer track 2 (of vector  
 421  $\vec{p}_2$ ) in a view a is given by:  
 422

$$\cos \theta = \frac{\vec{p}_1^a \cdot \vec{p}_2^a}{\|\vec{p}_1^a\| \|\vec{p}_2^a\|} \quad (1)$$

and the distance inter track is given by:

$$DIT = \|\vec{p}_1^a\| \sin \theta \quad (2)$$

423 The DIT should be higher than  $4 \times$  scintillator width for the track 1 to be not  
 424 superimposed with the track 2 in the view a, which also corresponds to 10.0 cm  
 425 in the nominal configuration.  
 426

### 7.1.2 Performances

427 The particle-only reconstruction efficiencies and the reconstruction threshold in momenta  
 428 are shown in Table 3. This threshold is defined as the maximal momentum for which the  
 429 reconstruction efficiency is smaller than 30%. The thresholds in muon and pion momenta  
 430 are 150 MeV/c. Most of the muons are above this threshold (see Figure 22) which leads  
 431 to a 79% reconstruction efficiency.  
 432

433 The lower pion and proton efficiencies (respectively 52% and 26%) are due to lower  
 434 efficiencies for similar momenta than muons, coming from strong interactions as shown  
 435 on Figures 24. Efficiencies of each particle type tend to decrease in the backward region  
 436

	$\mu$	$\pi$	p
Reconstruction Efficiency Momentum threshold	79% 150 MeV/c	52% 150 MeV/c	26% 550 MeV/c

Table 3: Reconstruction efficiency and momentum threshold for muons, pions and protons. The threshold is defined as the maximal momentum for which particles have a reconstruction efficiency smaller than 30%.

435 due to particle lower momenta. However, for a fixed momentum value, the reconstruction  
436 efficiency is almost uniform which confirms the ability of the WAGASCI detector to  
437 reconstruct high angle tracks.

438 The reconstruction is thereafter tested on neutrino events. Table 4 summarizes the  
439 number of reconstructed events and efficiencies for each interaction type. As expected  
440 from the high muon reconstruction efficiency, the charged current interactions have recon-  
struction efficiencies  $\geq 85\%$ .

	CC0 $\pi$	CC1 $\pi$	CCOthers	NC	All
Reconstruction efficiency	85%	87%	91%	22%	68%

Table 4: Number of true interactions reconstructed. The purity and reconstruction effi-  
ciency of each true interaction is also shown.

441  
442 The reconstruction efficiencies as a function of the neutrino energy and muon kinematics  
443 are respectively shown on Figure 25 and 26.

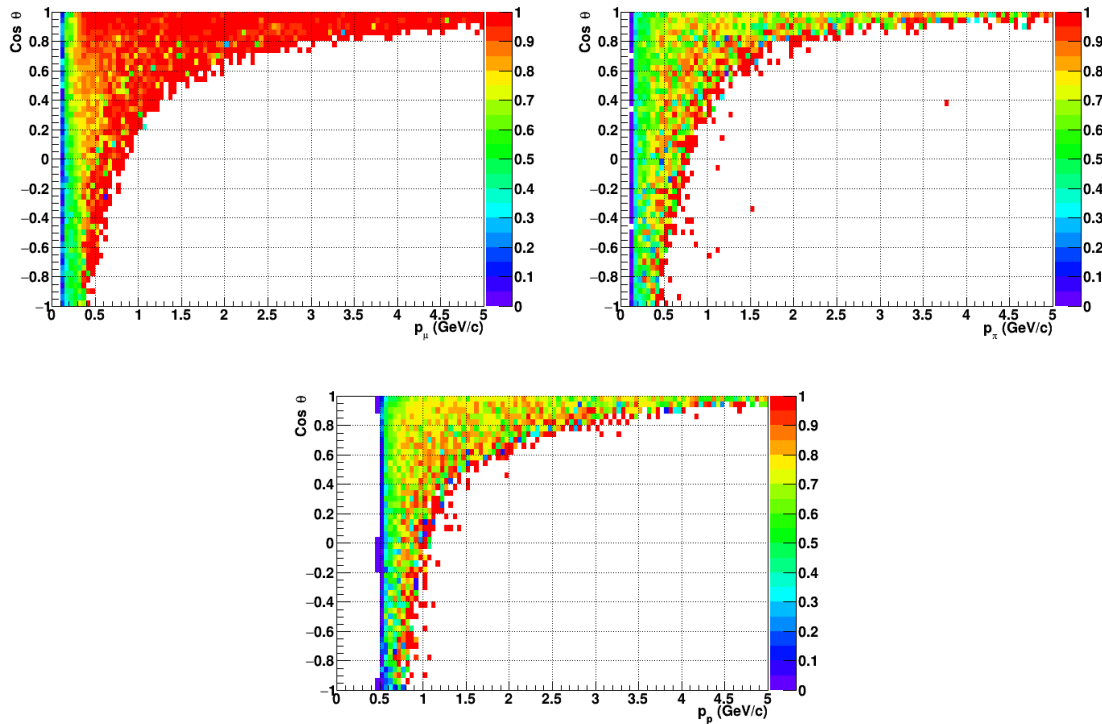


Figure 24: Reconstruction efficiency of muons (left), charged pions (right) and protons (bottom) in the WAGASCI water-module as a function of the particles momenta and angles.

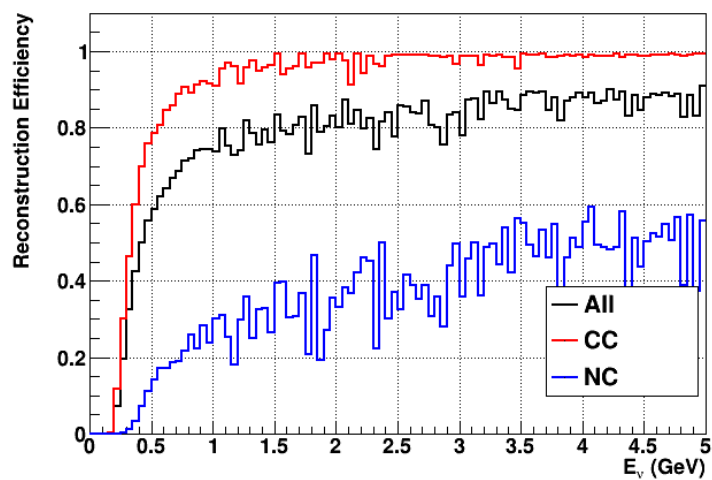


Figure 25: Reconstruction efficiency of all neutrino (black), CC (red) and NC (blue) interactions in the WAGASCI water-module as a function of the neutrino energy.

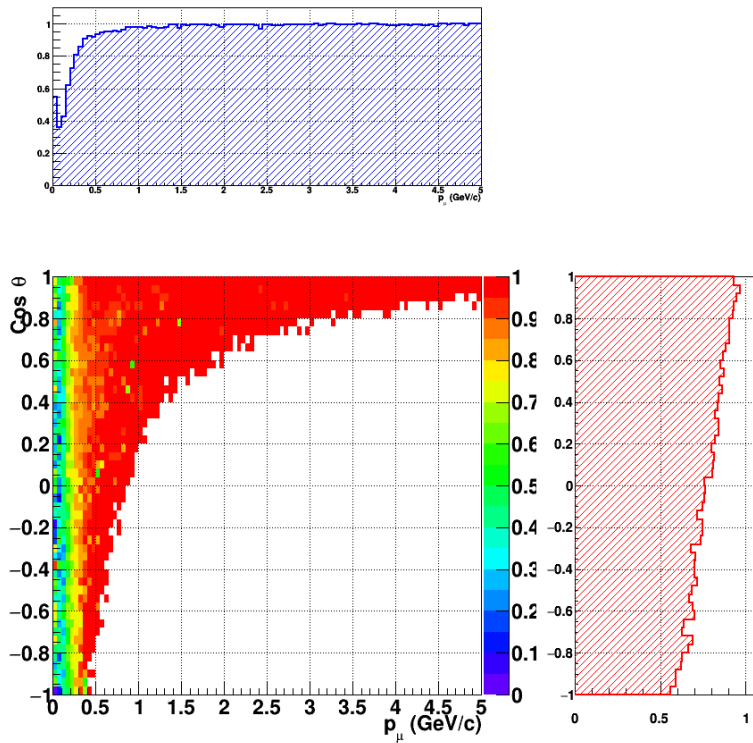


Figure 26: Reconstruction efficiency of CC interactions in the WAGASCI water-module as a function of the muon kinematic variables (momentum and angle).

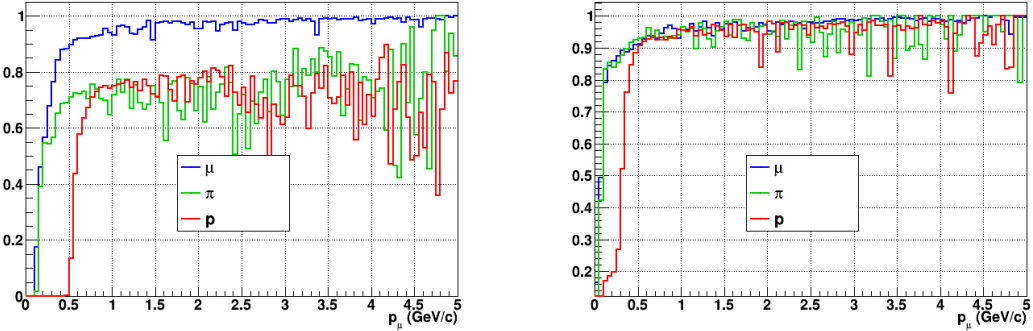


Figure 27: Reconstruction efficiency for muons, pions and protons in the water-in (left) and water-out (right) modules.

Note that a Particle Identification Algorithm has been also developed. It is based on the charge deposition of the particles in the scintillator, of the detection of a decay-electron. However, this information highly depends on the number of scintillator hit by a particle, which creates an important difference between a real WAGASCI module and the one used for the ND280-upgrade simulation. For this reason, the corresponding results will not be detailed here, but can be found in [?].

## 7.2 Background subtraction: the water-out module

In the nominal configuration, 20% of the neutrino interactions occurs on scintillators ( $C_8H_8$ ). This background should be removed in order to measure the neutrino interaction on the same target as Super-K, which suppress the differences in cross-section models. For this purpose, we propose to use a water-out module, where the water is replaced by air. The detector is therefore fully active and has a 3 mm spatial resolution (scintillator thickness) which create an ideal detector to reconstruct and identify hadrons, and study np-nh interactions. The counter-part is the difference in particle energy deposition between the water and this water-out module that will need to be corrected for. In this section, we present the capabilities of such a module, and the impact it can have on cross-section measurements for the neutrino community in general and T2K in particular. The same reconstruction and selection as the water-in module is applied. Figure 27 shows the comparison between the water-in and the water-out reconstruction efficiencies for muon, pions and protons. 90% of the muons and 87% of the pions are reconstructed, while 70% of the protons are even reconstructed. It allows to lower down the proton threshold to 250 MeV/c (see Table 5).

As a consequence of tracking even low momenta particle, the reconstruction efficiency is uniform and almost maximal on the entire  $\cos \theta_\mu$  phase space, as shown on Figure 28.

	$\mu$	$\pi$	p
Reconstruction Efficiency Momentum threshold	90% 50 MeV/c	87% 50 MeV/c	70% 250 MeV/c

Table 5: Reconstruction efficiency, proportions of  $\mu$ -like and non  $\mu$ -like and momentum threshold for muons, pions and protons in the empty module. The threshold is defined as the maximal momentum for which particles have a reconstruction efficiency smaller than 20%.

468 Since the fiducial mass represents 0.25 tons, the total number of events is divided by a  
 469 factor of 3 compared to the water-in module. The water-out module offers interesting  
 470 possibilities to study np-nh interaction since 70% of the protons are reconstructed. In the  
 471 future, a possible separation as a function of the number of proton track will be studied.  
 472 Moreover, we are currently pursuing the use of single and double transverse variables (cite  
 473 Xianguo) to open new possibilities for separating np-nh from Final State Interactions, or  
 474 for isolating the interactions on hydrogen from interactions on carbon in this module.

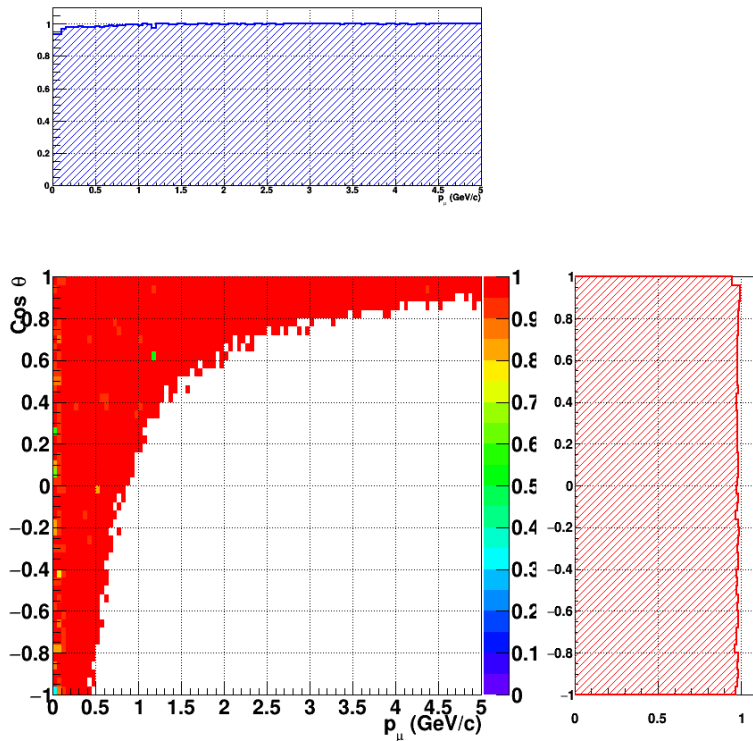


Figure 28: Reconstruction efficiency of CC interactions in the WAGASCI empty module as a function of the muon kinematic variables (momentum and angle).

475 **8 Schedule**

476 We would like to start a physics data taking from T2K beam time after the summer  
477 shutdown in 2018. By then, commissioning and tests of the detectors will be completed  
478 in J-PARC T59. The experiment can run parasitically with T2K, therefore we request no  
479 dedicated beam time nor beam condition as discussed in the following section.

480 Once the approved POT is accumulated, the WAGASCI modules will be removed  
481 from the experimental site, but we would like to keep the Baby-MIND and the Side-MRD  
482 modules on the B2 floor of the NM pit as common platforms of future neutrino experiments  
483 using the T2K neutrino beam.

484 **9 Requests**

485 **9.1 Neutrino beam**

486 The experiment can run parasitically with T2K, therefore we request no dedicated beam  
487 time nor beam condition. As data taking periods, we request the ‘nominal’ T2K one-year  
488 operation both for the neutrino beam and the antineutrino beam. The T2K has been  
489 requesting  $0.9 \times 10^{21}$  POT/year and actually accumulating about  $0.7 \times 10^{21}$  POT/year in  
490 recent years. For each year, starting from the Autumn, T2K is running predominantly in  
491 the neutrino mode or in the antineutrino mode. Our request is to have one-year neutrino-  
492 mode data and another one-year antineutrino mode data assuming that the POT for the  
493 fast extraction in each year is more than  $0.5 \times 10^{21}$  POT.

494 **9.2 Equipment request including power line**

495 We request the followings in terms of equipment on the B2 floor:

- 496 • Site for the WAGASCI modules, Side-MRD modules and BabyMIND and their elec-  
497 tronics system on the B2 floor of the near detector hall (Fig. 2).
- 498 • Anchor points (holes) on the B2 floor to secure the WAGASCI modules, Side-MRD  
499 module and Baby-MIND (Fig. ??)
- 500 • Power line for the magnets in Baby-MIND: 400 V tri-phase 48-to-62 Hz, capable of  
501 delivering 12 kW.
- 502 • Electricity for electronics and water circulation system, 3 kW, standard Japanese  
503 electrical sockets.
- 504     1. Online PCs: 2.1 kW
- 505     2. Electronics: 0.7 kW
- 506     3. Water sensors: ?

- 507     • Air conditioner for cooling heat generation at Baby-MIND magnets, online PCs and  
508       electronics
- 509     • Beam timing signal and spill information
- 510     • Network connection

511   **10 Conclusion**